Interfacial Failure Mechanism of 316LSS Diffusion Bonded Joints

Shu-Xin Li[1]*, Fu-Zhen Xuan[2], Shan-Tung Tu[2], Shu-Rong Yu[1]

[1] School of Petrochemical Engineering, Lanzhou University of Technology, Lanzhou, China;[2] School of Mechanical and Power Engineering, East China University of Science & Technology, Shanghai, China

Abstract

Diffusion bonding has been gaining greater attention in the fabrication of bonded joints of similar and dissimilar of austenitic stainless steel in nuclear and chemical industries, particularly in Micro Chemo Mechanical Systems. In situ observation of interfacial crack initiation and propagation was carried out on 316LSS vacuum diffusion bonded joints to investigate the microstructure evolution and effect of micro-voids on interfacial failure mechanism. The results showed that the most likely sites for cracks initiation are grain boundaries. The favorable grain boundaries containing cracks are oriented at 0º~20º to the loading axis. Intergranular cracks play a dominant role in interfacial failure. Micro-voids do not link up each other until the load is increased to 352MPa (63%σ_b). For 316LSS diffusion bonded joints, lots of experimental observations showed that interfacial failure depends mainly on microstructures of joints instead of micro-voids left on interface. This information may provide us an important insight to improve microstructures of joints after diffusion bonding.

Keywords: Diffusion bonded joints; Interfacial failure; Micro-voids.

1. Introduction

As one of the advanced material joining techniques, diffusion bonding has been gaining greater attention in the fabrication of bonded joints of similar and dissimilar of austenitic stainless steel in nuclear and chemical industries [1,2]. Diffusion bonding technique was also employed for making components in Micro Mechanical Systems, particularly the Micro Chemo Mechanical Systems [3], where conventional fusion welding is not appropriate for the microminiaturized structures and components, like compact intermediate heat exchanger for next-generation high temperature gas-cooled reactor [4].

Many works have been carried out on diffusion bonded joints of alloy-316LNSS or alloy-304SS. Ghosh et al [5,6] discussed solid-state diffusion bonding of titanium to 304 stainless steel and effect of interface microstructure on the bond strength was analyzed. It was reported that bond strength decreases with increasing bonding temperature due to increase in thickness of intermetallics.

Kundu and Chatterjee [7] studied diffusion-bonded joints between titanium and stainless steel with nickel as an intermediate material. Diffusion bonded joints of different materials to austenitic stainless steel were produced like Cu–Cr–Zr alloy [8] and Zirconia [9]. Nishi [10,11] studied the fatigue fracture behavior on diffusion bonded joints of alumina dispersion-strengthened copper (DSCu) to 316SS both experimentally and theoretically. A good agreement was observed between the measured and predicted results. Sato[12,13] discussed tensile and fatigue properties for Hot Isostatic Pressing (HIP) bonded joints of 316LSS and DSCu under optimum bonding condition. Marois [14] also discussed the joining of 316LSS to DSCu by HIP. The joint quality was assessed by tensile and fatigue testing at room temperature and 300°C.

However, the previous studies focused on macro mechanical behavior of diffusion bonded joints. Joints were evaluated by tensile, shear and fatigue properties. The microstructure evolution and interfacial deformation mechanism have not been seen for similar diffusion bonded joints of austenitic stainless steel. In our previous work [15], In situ observation of fatigue crack growth was carried out on bonded joints with discrete micro-voids located ahead of a pre-existing crack tip. The interfacial fatigue crack growth behavior was investigated. In the present study, microscopic tensile test is conducted on 316LSS diffusion bonded joints. Emphasis is laid on investigating interfacial failure mechanism and micro-voids evolution.

2. Experimental procedures

The material used in this study was cold-worked 316LSS having the following chemical composition in wt%: C-0.01, Si-0.41, Mn-1.41, P-0.036, S-0.006, Ni-12.43, Cr-17.84, Mo-2.16, Fe-balance. Solid state bonding was carried out in a vacuum diffusion bonding equipment with a vacuum of 1.33×10^{-3} Pa. In order to optimize the three main joining parameters (temperature, pressure and holding time), a series of diffusion bonding tests were conducted under the conditions of temperature of 1050°C-1100°C, the pressure of 7MPa-10MPa and the holding time of 2h-5h [16]. Tensile tests and Charpy impact at room temperature were carried out after bonding. It was found that the good joint was obtained under the condition of temperature 1100°C, pressure 10MPa and holding time 3h.

After joining, detailed metallographic inspections were conducted near the interface of diffusion bonded joints of 316LSS/316LSS. Micro-hardness was measured on the same specimen with Vickers micro-hardness. Three repeated tensile tests were conducted according to the Chinese Standard GB/T228-2002 with a testing machine (INSTRON 8800) at room temperature. The average ultimate tensile strength 566MPa (about 93.6%σ_{b1}, σ_{b1} is the ultimate tensile strength of parent material), yield strength 210MPa and section shrinkage rate Ψ

28%. The repeatability in the mechanical response was good with only minor variations.

2.1 In situ tensile test

The tensile specimens were manufactured with the joint interface at the center, shown in Fig.1. All specimens were metallographically polished and etched to obtain appearance of metallographic structure. The tests were performed by applying a micro-fatigue testing device [15] at room temperature. The axial tension loading was perpendicular to the interface. The specimen was loaded step by step in order to observe microstructure evolution.

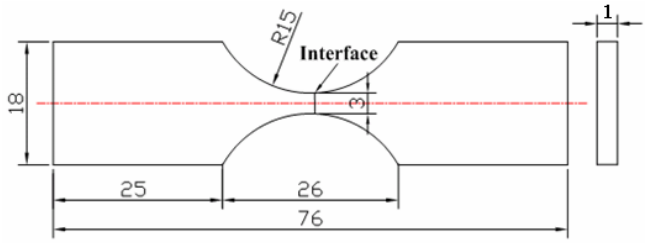

Fig.1 Shape and dimensions of the microscopic tensile specimen (mm)

2.2 In situ fatigue test

Single edge-notched fatigue specimen was employed in fatigue test. For single edge-notched specimen, the specimen was manufactured with notch at the interface. The fatigue tests were performed at room temperature under load control at R=0.1, with a sine waveform of 0.5 Hz frequency. The axial tension-tension loading was perpendicular to the interface. The maximum load amplitude is 500N (215MP, 38% σ_{b2} is the ultimate tensile strength of joints). The test was paused after a number of cycles in order to take and save pictures, with the load holding at the average stress, and then restarted.

3. Results and discussion

3.1 Interface characteristics

The optical micrographs of joints near the interface are shown in Fig.2. It can be seen that no obvious bonding line was observed on the interface and the percentage of bonded area was more than 90%. The interface itself is indeed grain boundary due to formation of metallic bond between atoms on each surface in diffusion bonding. Only a few micro-voids scatter on the interface. But here, we still call it interface in order to distinguish from grain boundaries of parent materials.

The high temperature promotes serious grain coarsening. The grain size is unevenly distributed varying from 20μm to 160μm and some grains are even larger, shown in Fig.3. Meanwhile, large amounts of annealing twins are observed

in joints. Coarsening grains and annealing twins cause the decrease of ductility in joints. This can explain why the section shrinkage rate of joints is only 40% of that of parent material.

The Vickers micro-hardness was measured through traverse perpendicular to the bonding line, under the conditions of loading of 100g and the holding time of 15 seconds, shown in Fig.4. No significant differences were detected in micro-hardness between different measured points near the bonding line.

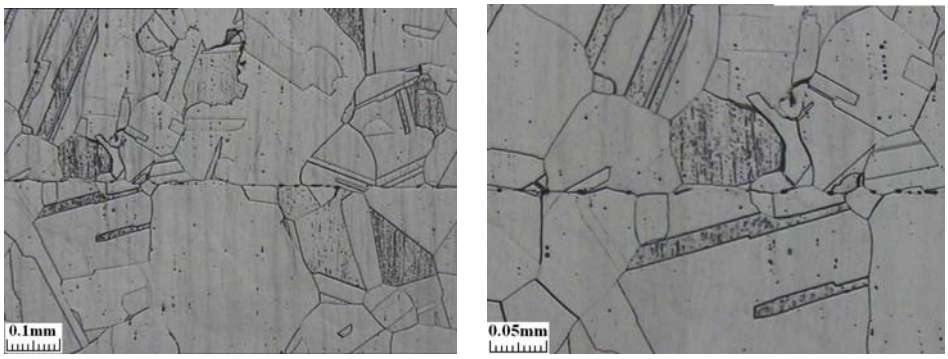

Fig.2 Microstructure of bonded joint

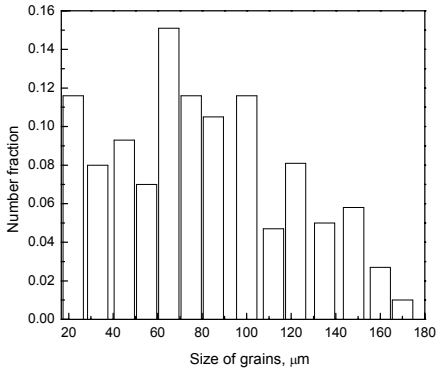

Fig.3 Distribution of grain size of bonded joints

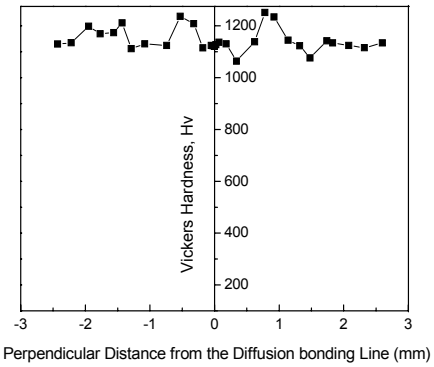

Fig.4 Vickers micro-hardness of bonded joint

3.2. Results of in situ tensile test

3.2.1 Crack initiation and propagation

Figs.5(a)-(d) shows the interfacial failure process of 316LSS bonded joints under different stresses at the same place. Fig.5(e) shows the microscopic deformation of the specimen at stress of 520MPa. The specimen fractured at the interface with ultimate tensile strength of 556MPa. The in situ observation of microstructure evolution revealed that crack nucleation occurs from slip bands, grain boundaries (GBs) and interfacial micro-voids.

In the microscopic tensile test, slip lines could be seen clearly in grains when the

stress exceeded yield stress. They were orientated along maximum shear stress direction 45º and parallel to the loading axis, as indicated by arrows in Fig.5(a) . When the load exceeded 400MPa, serious plastic deformation occurred and the strongly deformed sample was buckled, as shown in Fig.5(b). In addition, Lots of small cracks initiated and propagated simultaneously at slip bands in the same grain, particular in large grains, as seen clearly in Fig.5(e).

From our observation the most likely sites for crack initiation are grain boundaries. The angle between cracked GBs and loading axis is 0º~20º. Some of them are parallel to the loading axis, as shown by arrows in Fig.5(b) and Fig.5(e). For GBs far away from interface, cracks initiated at these grain boundaries by slip bands impinging against GBs, as marked with "A" in Fig.5(e). In most cases, large grains with grain boundaries almost parallel to loading axis are preferable for intergranular crack initiation. Long GBs had little obstruction on crack growth. Once intergranular cracks were observed, they extended quickly but straightly along GBs towards the interface, without branching and deflecting. For GBs adjacent to interfacial micro-voids, micro-voids induced cracks and then propagate along GBs preferably, thus forming intergranular cracks, as marked with "B" in Fig.5(c) and Fig.5(e).

3.2.2 Micro-voids evolution

At the same stress level, surface observation showed that the deformation of grains was preferable to the change of micro-voids. Micro-cracks induced by local stress concentration at the tip of micro-voids propagated along interface to coalesce with adjacent micro-voids. But this was only in the case where driving force was big enough for initiation of micro-cracks. In the test, when the specimen was loaded at 400MPa, shown in Fig.5(b), much plastic deformation has occurred in grains, while micro-voids became wider correspondingly but did not propagate along the interface. Under the magnification of 1000X, micro-voids and micro-voids did not coalesce until the stress exceeded 352MPa. When the stress was increased to 400MPa (72%σ_b), several micro-voids linked up with each other to form a longer interfacial crack. Therefore, it can be inferred that if load is kept at certain level, no coalescence of micro-voids and micro-voids will occur.

Repeated tests showed that compared to micro-voids, grain boundaries are places where cracks initiate and propagate easily. The main reason is probably that those interfacial micro-voids are blunt due to surface diffusion mechanism in diffusion bonding, which requires large driving force for crack initiation. Meanwhile, grain boundaries located at micro-voids are more favorable for crack initiation and propagation.

From Fig.5(b) to Fig.5(d), the stress between 400MPa and 550MPa, microstructure of the surface had no major change except strengthening slip bands and widening cracks. In this stage, cracks extended through the specimen's thickness. There was no main crack formed during the whole failure process.

Cracks originated from slip bands, micro-voids particularly grain boundaries weakened the specimen and thus caused fracture. In fact, the observed part from Fig.5(a) to Fig.5(d) is the weakest section of the specimen. The coalescence of interfacial micro-voids at the large grain marked “A” results in debonding of the grain and interface. Its grain boundaries parallel to the loading axis are favorably oriented grain boundaries where cracks nucleated. Thus, fracture occurred at this place first.

The overall grain deformation showed that intergranular cracks are the main contributor for interfacial failure. The interface was weakened seriously by lots of cracked grain boundaries and then fractured when the section was not able to sustain the load. Therefore, for 316LSS diffusion bonded joints, microstructure plays an important role in interfacial failure. This information may provide us an important insight to improve microstructures of joints after diffusion bonding.

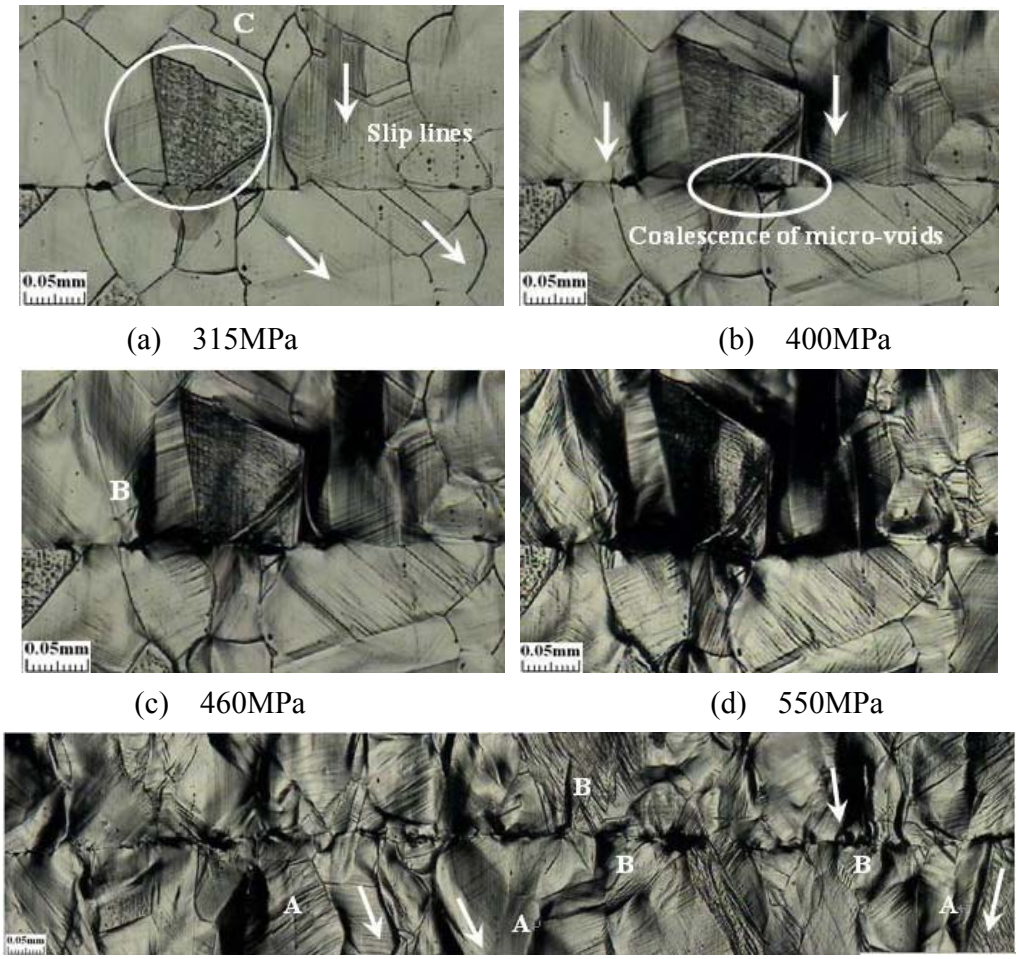

(a) 315MPa (b) 400MPa

(c) 460MPa (d) 550MPa

(e) 520MPa

Fig. 5 Interfacial failure process of bonded joints: (a) 315MPa, (b) 400MPa, (c) 460MPa, (d) 550MPa, (e) 520MPa

3.3. Results of in situ fatigue test

3.3.1 Interfacial fatigue crack initiation and propagation

Fig.6 shows the evolution of the interfacial crack and micro-voids from 20000 cycles to 30000 cycles. The fatigue life of this specimen is 30350 cycles. For clear interpretation, cracks and micro-voids were labeled with capital letters in Fig.6 since there is more than one crack produced in the fatigue loading, with the main crack labeling A. Crack initiated at the upper side of the interface. When the cycles reached 20000, the crack has grown 0.006mm and advanced towards the interface in 60º direction with the interface, shown in Fig.6 a (N=20000). The crack proceeded until the crack tip met the interface. Then it coalesced with the micro-void B, developing the main crack A, Fig.6 b (N=22175).

The interface ahead of the micro-void C is ridge-like rather than straight, Fig.6 b. In diffusion bonding, a ridge interface is formed when the two convex surfaces contact. The size of ridge is therefore determined by the surface roughness.

The main crack did not propagate along the interface after it passed through the micro-void C. Instead, it changed the direction and grew on the symmetrically opposite direction of ridge, forming the crack D, shown in Fig.6 c (N=24288). The crack D seemed to become the main crack. However, a new crack E produced at the symmetric location of the right side of ridge and grew towards the interface, Fig.6 c. In subsequent propagation it became the main crack. Meanwhile, the crack E stopped propagating and arrested at the grain, Fig.6 d (N=25000). It is worth noting that, in this region, the crack became transgranular rather than propagated along the interface. As the crack extended, the crack coalesced with the micro-void F immediately, causing a jump-like increase in the crack length, which accelerated the crack growth process.

It can be seen in Fig.6 e (N=25500) that the main crack extended along the left side of ridge interface, but impeded by the grain boundary ahead. In fact, the ridge interface can resist the crack propagation, namely reduces crack propagation rate to a certain degree. The reason is probably that crack propagation is under mixed-mode loading since the ridge interface is at certain inclination angle to the loading. Therefore, the fatigue crack propagation on the interface is influenced not only by the loading and material properties, but the asperity of the interface as well.

The transgranular crack growth can be seen clearly in Fig.6 f (N=26500). The main crack A deflected the interface and extended through the grain, forming crack G. Unexpectedly, a new crack I appeared at the crack tip and advanced towards interface. It coalesced with the micro-void when met the interface, Fig.6 g (N=27500). In subsequent propagation, the main crack deviated the interface and turned to transgranular growth, Fig.6 h (N=28000), forming a wavy path. An interesting thing during the crack growth was that: the transgranular crack grew no more than 0.05mm. Then it returned back to the interface. The same

phenomenon was also found in Fig.6s e and h.

As the test proceeded, the stress increased due to the decrease of the specimen section, and eventually the instability of crack growth leads to the final fracture. From the whole process of crack propagation, we can see that the main crack growth follows a wavy path and exhibits multi-path options: transgranular, intergranular or near the interface.

3.3.2 Fatigue failure mechanism of 316LSS diffusion bonded joints

The micro-void H grew simultaneously as the crack proceeded, shown in Fig.6 i (N=29500). Its coalescence with the main crack resulted in a fast increase in the growth rate. The phenomenon is very exceptional in the test. Under the magnification 1000X, a number of repeated tests showed that no size and shape change of the micro-voids ahead of the crack was observed as the crack advanced. For example, the micro-void J (Fig.6 h) had no any change after 28000 cycles, even if the grain adjacent to the micro-void J has deformed obviously, shown in Fig.6 h.

For the joints of dissimilar materials with discrete interfacial micro-voids located ahead of a crack, the mechanisms of interfacial failure have been accounted for by the following way [17-20]: (1) crack initiation at micro-voids (2) micro-voids growth (3) coalescence of crack and micro-voids (4) coalescence of micro-voids and micro-voids. The process repeats until the crack comes into instable growth and fracture occurs. However, for 316LSS/316LSS joints, the micro-voids ahead of the crack were unchanged as the crack proceeded and no coalescence of micro-voids and micro-voids was observed during the repeated tests. Therefore, the fatigue failure mechanism of similar diffusion bonded joints is different from that of joints of dissimilar materials.

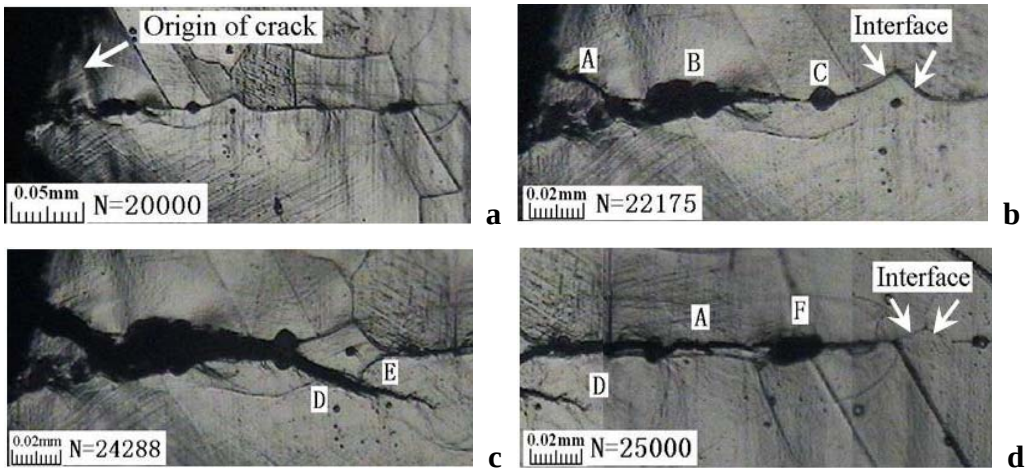

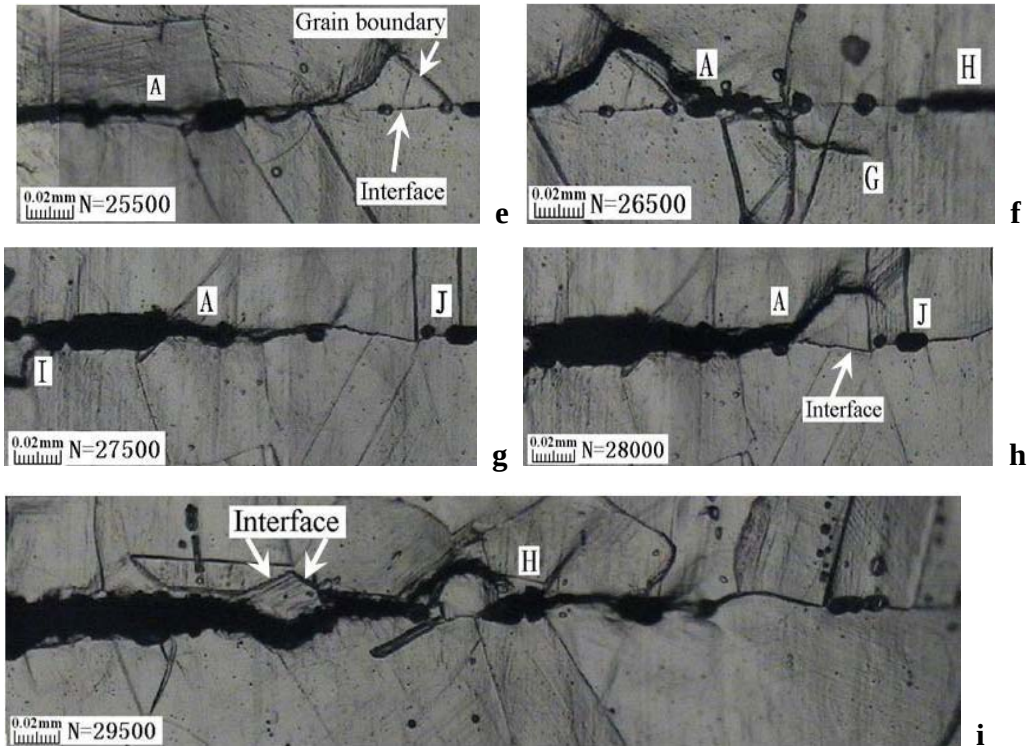

Fig.6 Evolution of the interfacial fatigue crack and micro-voids

4. Conclusions

(1) The high temperature promotes serious grain coarsening in 316LSS diffusion bonded joints. The coarsening grains and large amounts of annealing twins provide the main contributions to the decrease of ductility in joints.

(2) Compared to interfacial micro-voids, grain boundaries are places where cracks initiate and propagate easily. The favorably cracked grain boundaries were oriented at 0º~20º to the loading axis. Under the magnification of 1000X, micro-voids and micro-voids do not coalesce until the load is increased to 352MPa (63%σ_b). Micro-voids left on interface are blunt due to surface diffusion mechanism in diffusion bonding, which requires large driving force for crack initiation. For 316LSS diffusion bonded joints, interfacial failure depends mainly on microstructures of joints instead of micro-voids left on interface.

(3) No size and shape changes of the micro-voids are observed as the fatigue crack propagates though the appreciable plastic deformation occurs in grains adjacent to the fatigue crack tip. The main fatigue crack growth follows a wavy path and exhibits multi-path options: transgranular, intergranular or near the interface. The fatigue crack propagation is influenced not only by the loading and material properties, but by the roughness of the interface as well.

Acknowledgements

The authors are grateful for the supports provided by China Natural Science Foundation (50805072), Gansu Province Natural Science Foundation (2008GS02589) and PHD Foundation of Lanzhou University of Science and Technology(SB05200801). FZ would also wish to thank the supports provided by Shanghai Rising-Star Program (05QMX1416).

References

[1] H. Kato, S. Abe, T. Tomizawa, J. Mater. Sci. 32 (1997) 5225–5232.
[2] B.C. Odegard, B.A. Kalin, J. Nucl. Mater. 233-237 (1996) 44-50.
[3] K. Takahashi , M. Umemoto, N. Tanaka, Microelectronics Reliability, 43(8) (2003) 1267-1279.
[4] T. Takeda, K. Kunitomi, T. Horie. Nucl. Eng. Design. 168 (1997) 11-21.
[5] M. Ghosh, K. Bhanumurthy, G. B. Kale, J. Krishnan and S. Chatterjee. J. Nucl. Mater. 322 (2003) 235-241.
[6] M. Ghosh, D. Samar, P. S. Banarjee and S. Chatterjeea. Mater. Sci. Eng. A 390 (2005) 217-226.
[7] S. Kundu, M Ghosh, A Laik, G.B. Kale and S. Chatterjee. Mater. Sci. Eng. A 407 (2005) 154–160.
[8] I. S. Batra, G. B. Kale, T. K. Saha, Mater. Sci. Eng. A 369 (2004) 119-123.
[9] R. H. Vegter, A. T. J. V. Helvoort, G. D. Ouden, J. Advanced Mater. 35 (2003) 17-24.
[10] H. Nishi, T. Araki, J. Nucl. Mater. 283-287 (2000) 1234-1237.
[11] H. Nishi, J. Nucl. Mater. 329-333 (2004) 1567-1570.
[12] S. Sato, T. Kuroda, T. Kurasawa, J. Nucl. Mater. 233-237 (1996) 940-944.
[13] S. Sato, T. Hatano, T. Kurasawa, J. Nucl. Mater. 258-263 (1998) 265-270.
[14] G. L. Marois, H. Burlet, R. Solomon, Fusion Eng. Des. 39-40 (1998) 253-261.
[15] S. X. Li, F. Z. Xuan, S. T. Tu, J. Nucl. Mater, 366 (2007) 1-7.
[16] Z. L. An, W. L. Luan, F. Z. Xuan, S. T. Tu, Key Eng. Mater. 297-300(2005): 2795-2804.
[17] E. K. Tschegg, H. O. K. Kirchner, M. Kocak, Acta Metall. Mater. 38(3) (1990) 469-478.
[18] R. M. Cannon, B. J. Dalgleish, R. H. Dauskardt. Acta Metall. Mater. 39(9) (1991) 2145-2156.
[19] C. Woeltjen, C. F. Shih, S. Suresh, Acta Metall. Mater. 41(8) (1993) 2317-2335.
[20] M. R. Turner, A. G. Evans, Acta Mater. 44(3) (1996) 863-871.